frontiers | Frontiers in Earth Science

TYPE Original Research
PUBLISHED 02 February 2023
DOI 10.3389/feart.2022.1114292

OPEN ACCESS

EDITED BY
Naifei Liu,
Xi'an University of Architecture and Technology, China

REVIEWED BY
Zhong Han,
Wuhan University, China
Shunchao Qi,
Sichuan University, China

*CORRESPONDENCE
Zhang Hongri,
253541461@qq.com

SPECIALTY SECTION
This article was submitted to Environmental Informatics and Remote Sensing,
a section of the journal
Frontiers in Earth Science

RECEIVED 02 December 2022
ACCEPTED 28 December 2022
PUBLISHED 02 February 2023

CITATION
Youjun L, Hongri Z, Liming H, Sulian L, Hongming L and Xuexiao W (2023), Reaction and deformation mechanism of a slipping-stretching landslide: Example of the Liangtianao ancient landslide, Guangxi Province, China.
Front. Earth Sci. 10:1114292.
doi: 10.3389/feart.2022.1114292

Reaction and deformation mechanism of a slipping-stretching landslide: Example of the Liangtianao ancient landslide, Guangxi Province, China

Li Youjun[1], Zhang Hongri[1,2]*, Huang Liming[1], Lan Sulian[3], Li Hongming[1] and Wu Xuexiao[1]

[1]Guangxi Transportation Science and Technology Group Co., Ltd., Nanning, Guangxi, China, [2]School of Naval Architecture, Ocean & Civil Engineering, Shanghai Jiaotong University, Shanghai, China, [3]Guangxi Transport Vocational and Technical College, Nanning, Guangxi, China

Slipping-stretching landslides have long been recognized as a common type of landslide case, but such reactions have rarely been reported. There was a slipping-stretching landslide reaction at Liangtianao, Guangxi Province, China, and the geological background and deformation characteristics of the case were identified by detailed geological survey and long-term monitoring. A FEM model of the case was built using GEO5 to analyze the mechanism of reaction and deformation. The results are as follows. 1) The Liangtianao landslide is a bedding rock ancient landslide, which remained in a creeping state after the landslide occurred in geological history. 2) The new sliding surface in the Liangtianao landslide is basically consistent with the weak interlayers formed by ancient landslides, and the fault-type is a slipping-stretching type with the following deformation process: strain at leading edge by road excavation→ leading edge instability→ middle part shear and creep→ back edge tensile. 3) Micro-geomorphology, rock mass bedding, and weak interlayers are internal causes of the Liangtianao landslide reaction, while excavation unloading and rainfall are the external causes. The inclinometer indicates that the Liangtianao landslide is still highly sensitive to rainfall after the landslide reaction, which may trigger a secondary landslide reaction. 4) The numerical analysis results indicate that the maintenance of a passive state in the anti-sliding section is highly beneficial to maintaining basic stability after the landslide reaction; unloading only 1/20 of the sliding section makes the landslide stable in the long term.

KEYWORDS

landslide reaction mechanism, deformation mechanism, slipping-stretching landslide, unloading effect, rainfall touch-slip effect, deformation characteristics, secondary reaction

1 Introduction

As the frequency of human engineering activities and extreme weather increase, reaction cases of ancient landslides are increasing. Landslides in British Columbia have moved to the Thompson River Valley, posing a threat to the Canadian Pacific Railway and the Canadian National Railway (Macciotta et al., 2016). The OSO landslide in Washington, D.C. has been studied for decades, but its reaction had still not stopped in 2014 (Wartman et al., 2016). The retreat of the Barry Glacier has exposed many ancient landslides in southern Alaska, which pose potentially disastrous consequences if these landslides enter the fjord in reaction, raising

questions about its stability and potential cascade hazards (Wolken et al., 2021). Therefore, it is especially important to study the reaction mechanism of ancient landslides.

Slipping-stretching landslides activate a bedding sliding section in their middle-upper part and a passive compression section in their lower part. Under the action of gravity, the middle-upper part slides along the weak interlayer zone, and the lower part produces passive extrusion. When the interlayer weak zone in the lower part cannot sufficiently maintain passive extrusion, the sliding surface penetrates and slides. The presence of rock strata and the properties of the interlayer zone are the main controlling factors for such landslides, and are considered a common type of landslide (Broadbent and Ko, 1971; Lo et al., 1978). Huang (2009) summarized the main characteristics of such landslides, and proposed that they are mainly induced by rainfall and weak interlayers. Li M et al. (2008) proposed that bedrock bedding landslides have a weak slide face at the interlaminar shear band stage, and are prone to forming new disasters. Li X et al. (2008) proposed that the range of monoclinic bedrock ancient landslides obtained from geomorphological analysis had multiple causes. Zhang (2016) researched the process of slipping-stretching landslides; because the pull-cracks located at landslide trailing were directly connected to the slip surface, the influence of rainfall on landslide stability required special attention. Burda et al. (2013) proposed that continuous underground mining and rainfall had induced the secondary reaction of the Eisenberg ancient landslide in northern Bohemia. Deng et al. (2017) indicated that the unloading effect caused by river down-cutting had gradually penetrated the formation process of ancient landslides, complex landslides, and multi-level landslides. Song et al. (2012), Huang et al. (2013), Zou et al. (2012), Chen et al. (2014), Xue et al. (2015), , Qu et al. (2016), Wu et al. (2018), Wei et al. (2018), Huang et al. (2020), Zhang X et al. (2021), Zhong et al. (2021), and Zhang et al. (2022) have proposed that bottom unloading and heavy rainfall cause weight gain and shear-strength weakening, which promote ancient landslide reaction. Wei et al. (2018) and Sangirardi et al. (2020) observed that unloading at the slope foot is a common inducement for ancient landslide reactions. Liu et al. (2023) concluded that rock fractures cracked significantly at low temperatures. CaiI et al. (2021) concluded that the Diexi earthquake in 1933 triggered tension cracks in the Xinmo landslide and that long-term rainfall caused landslide reaction. Deng et al. (2017) conducted the Brazilian splitting test on slate under different bedding angles θ, and observed that the slipping-stretching landslide mode appeared when $30^{\circ} < \theta < 45^{\circ}$. Zhang C et al. (2021) concluded, based on the centrifuge physical model test and numerical simulation, that a dominant infiltration channel formed by cracks was necessary for aggravating geotechnical mixed ancient landslide reactions. Pradhan et al. (2022) concluded that road cuttings increased landslides during rainfall and decreased minimum starting rainfall. Zhang C et al. (2021) found that the hydraulic gradient was the most important factor for the Taping landslide. Liu et al. (2022) concluded that rock degradation was caused by freeze–thaw cycles, and that this degradation or loss of strength could cause damage when the rock was thawed. According to all this research, unloading, loading, rainfall, earthquake, and bad lithology are the main factors for ancient landslide reaction. As the slipping-stretching landslides are regularly reported, exploring such landslides' deformation characteristics and reaction mechanisms is beneficial for reducing the loss they cause.

There was a slipping-stretching landslide reaction in Liangtianao, Guangxi Province, China. The deformation characteristics, evolution process, cause analysis, and reaction characteristics were evaluated by geological drilling, geotechnical testing, long-term deep displacement monitoring, and numerical analysis. The reaction and deformation mechanisms of the landslide were analyzed by daily rainfall, monitoring data, and numerical modeling. The principles of this landslide are discussed in this study to provide an analogy and prevention reference for similar ancient landslides.

2 Geological background of landslide area

This case is located at Tian'e country in Guangxi Province, China. The geomorphic type of the case area is mainly erosion dissolution low mountain valley landform (Figure 1). Its elevation is 800 m–1,450 m, and the valley bottom is a relatively open "V" shape with gradients of between 40 and 90°. Overall, the peak bridge fluctuates in waves, and the valley is shallow and wide in strips. The study area is in the Nandan fault zone of the Guixi sag, Youjiang regeneration geosyncline, Nanhua platform. Affected by the regional structure of the Tian'e anticline, the Bala-Longfeng normal fault (NW60°) developed along the left flank of the anticline; it has a steep wall of soft Middle Triassic rock, a the lower wall comprising rigid Middle Permian rock. The groundwater type of the case area is a poor amount of bedrock fissure water. Its climate is subtropical humid monsoon. Annual rainfall precipitation (1,370 mm) occurs in the wet season (May–October), and accounts for 85% of the rainfall throughout the year (Zhang et al., 2021b).

The case was in Liangtian'ao village (Figure 2). The G243 national way designed sections of K16 + 300 to K18 + 500 near this village. As the height difference between front and rear is 120 m, double-S turning curves were taken to overcome the longitudinal slope, with total excavation of these sections of 43,898 m^3. All excavation was completed in July 2018 and formed platforms 11 m–20 m wide at 757.0, 790.0, 818.0, and 833.0 m. Nearly 22 concrete- brick houses with 100 villagers are scattered on the top of the slope.

The main composition of the lithology is as follows. The surface layer is yellowish-brown quaternary residual silty clay, with a gravel content of 5%–10%,and an exposed thickness varying 0.5–6.0 m. The lower part is thin to medium thickness layered argillaceous siltstone, with an argillaceous silt structure and developed joints and fissures, exposed 5.0 m–45.0 m-thick. The rock mass occurrence is 260°∠26°.

3 Landslide features

3.1 Development of the landslide

The tongue-shaped landslide occurred suddenly on August 13, 2018, and its failure characteristics were as follows. a) At 870 m, the soil was separated from the steep rock wall behind it and slinked about 30 cm; at 860 m, three houses' load-bearing columns were cracked by 0.5 cm–1.0 cm. b) At 831 m–873 m, the shallow soil was stretched by 10 cm to 30 cm-thick, and the new retaining wall was staggered 10 cm–25 cm. c) At 790 m–818 m, the old road sustained goose-sharped shear dislocations, and the old retraining walls cracked diagonallly 1~2 cm wide. d) At 750 m–790 m, there was only slope slump outside the boundary on both sides, and the sliding surface was not exposed. In order to determine the spatial characteristics of this

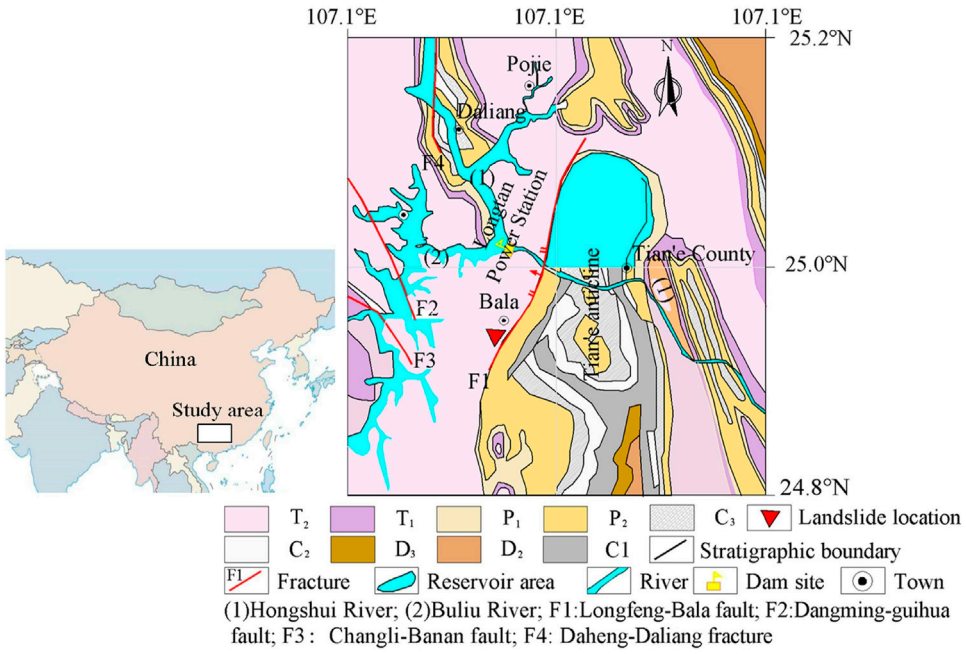

FIGURE 1
Geographical location map of landslide area.

landslide, three geological profiles were laid along the main direction, and deep displacement monitoring was set up. The specific layout positions and sliding surfaces are shown in Figures 2 and 3.

The plane of the landslide was tongue-shaped, with a narrow upper and a wider lower. The trailing edge was bounded by steep-standing soft Middle Triassic rock, with boundaries both sides of the U-shaped groove. The main shaft length was 220 m. The elevations of the front and rear edges were 760 and 880 m respectively, which is in the direction of the vertical main axis—the width varied 69 m–110 m. The average thickness of the sliding body was about 20 m, and landslide volume was about 250 × 10^3 m^3. The Liangtianao landslide was thus a medium-sized dipping thick bedrock landslide.

3.2 Relationship between landslides and rainfall

Pre-landslide rainfall was characterized by prolonged, high intensity (Figure 4). The cumulative rainfall from March 2018 to the landslide reached 2,137.0 mm, accounting for 70.3% of the whole year (3,040.0 mm). The average daily rainfall was up to 12.64 mm/d. Furthermore, the rain continued from 30 March 2018 to 12 August 2018 (11 days) before the landslide, with a large day rainfall of 72.6 mm on 11 August 2018. As all on-site works had stopped before the landslide occurred, it can be qualitatively judged that the rainfall contributed to the landslide.

After the landslide occurred, on-site construction was stopped until March 2019. However, the daily rainfall and deep cumulative displacement curve showed a continuous deformation trend, which was closely related to rainfall.

1) The slip gradually stabilized from the leading to the rear edge. After the landslide, the cumulative rainfall between 1 August 2018 and 19 September 2019 (39 days) was 634.6 mm, of which the average daily rainfall from 17 September 2019 to 19 September 2019 was 61.0 mm/d. Consequently, shallow soil at the trailing edge slipped 219°, causing the village road to dislocate (Figure 5). The dry season had been from 19 August 2018 to 31 March 2019, with cumulative rainfall down to 502.8 mm (2.60 mm/d). By comparison, the average daily evaporation in the region was 3.40 mm, so the rainfall effect on the landslide was weak. However, the middle sliding body was still slipping. The subsidence gap of the retaining wall near ZK2-6 cracked in October 2018 (Figure 6). Moreover, as deep displacement monitoring was completed on 21 November 2019, the average displacement rate of all sliding surfaces during the dry season was 0.08 mm/d, 0.15 mm/d, 0.12 mm/d, and 0.42 mm/d. This reveals that, 152 d after the landslide reaction, landslide had entered a gradual stabilized stage from its rear to upper edge.
2) Rainfall can cause landslides to re-deform. On 1 March 2019, there was no change in the deep displacement monitoring data after the deep drainage holes were completed. However, with the average daily rainfall reaching 5.48 mm/d (26 March 2019 to 30 April 2019), the cumulative displacement of the sliding surface at ZK2-3 suddenly increased from 18.7 mm to 34.85 mm (+16.15 mm). In contrast, the ZK2-6 cumulative displacement did not change.

3.2.1 Landslide deformation and rainfall distribution

There was good correspondence between landslide deformation and rainfall distribution. Continuous high-intensity rainfall can trigger a secondary landslide reaction.

3) Deformation failure feature. The ZK2-6 borehole at the front edge exposed two broken layers (Figure 3). The upper layer is

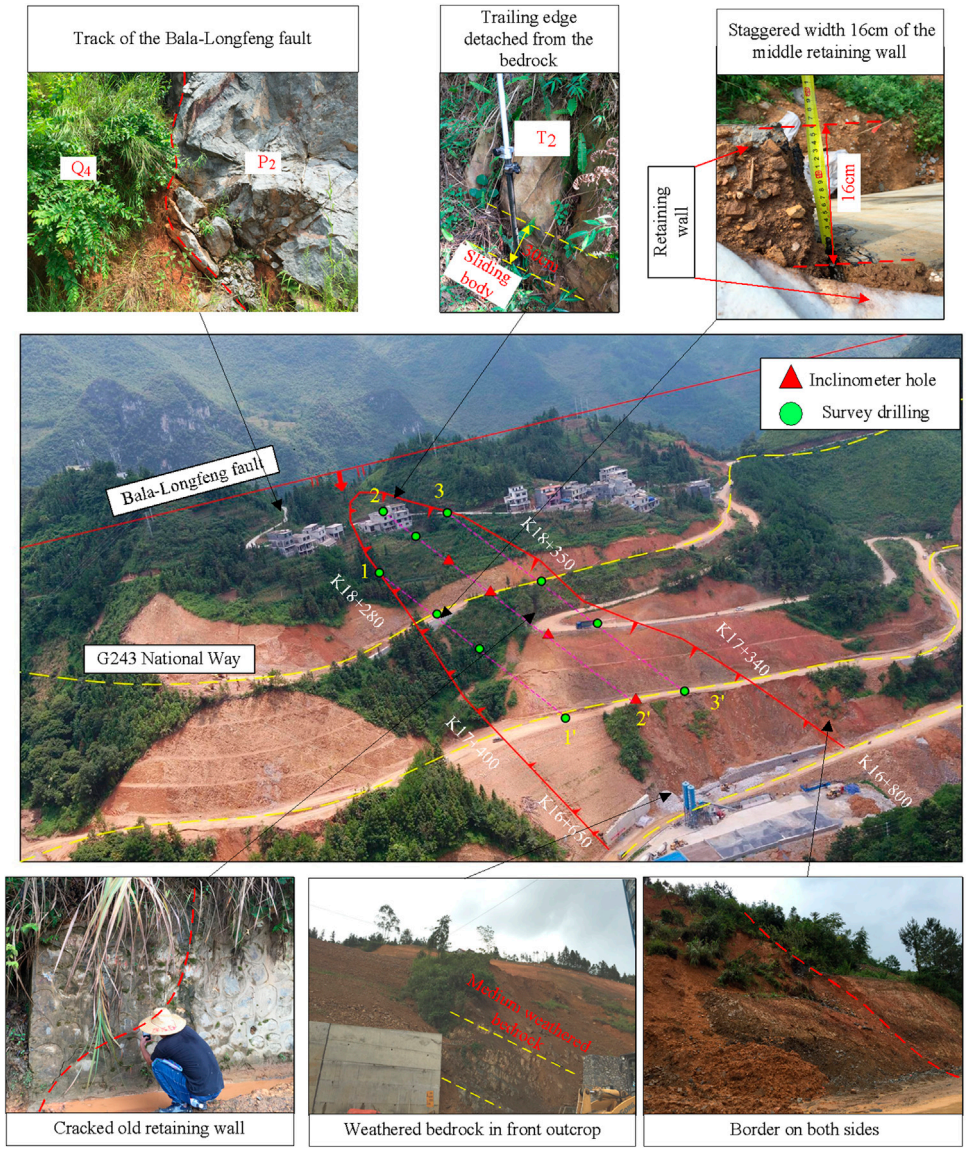

FIGURE 2
Landslide plan and typical damage photos (SE139°, August 2018).

composed of gravel-like yellow argillaceous siltstone, sub-angular and sub-circular, with a particle size of 3 ~ 5 cm. It contained 0.2–2.0 cm of loose sandy breccia—evidence of interlayer dislocation caused by ancient landsliding.

3.3 Identification of ancient landslide characteristics

The identification of ancient landslide characteristics in this case is mainly based on surface morphology, stratum lithology, deformation, and failure characteristics.

1) Geomorphic features of the study area. The original landform formed a gentle platform at 815 m to 818 m, each section having angles of 40°, 26°, and 50°. From top to bottom, the landform was steep–gentle–steep, with obvious grading, forming a typical chair-shaped landform. A 5 m-high steep rock wall appeared outside the boundary at the trailing edge of the landslide, which was formed when the rear part of the ancient landslide slipped.
2) Stratigraphic lithology. Longitudinally, rock formation is 260°∠26° in the upper part and 260°∠0° in the lower part, forming a gently dipping-out layered slope. At 100 m from the left of the landslide, the rock formation changed from 260°∠26° to 180°∠25°, and an obvious interlayer fracture zone with a thickness of 0.2–0.3 m was seen in the excavation face (Figure 7).
3) Deformation failure feature. The ZK2-6 borehole had exposed two broken layers (Figure 3). The upper layer was composed of soft argillaceous siltstone, sub-angular and sub-circular, with particle sizes 3 cm–5 cm and contained 0.2 cm–2.0 cm thickness of loose sandy breccia, which belonged to the basis of the interlayer dislocation caused by ancient landslides in geological history.

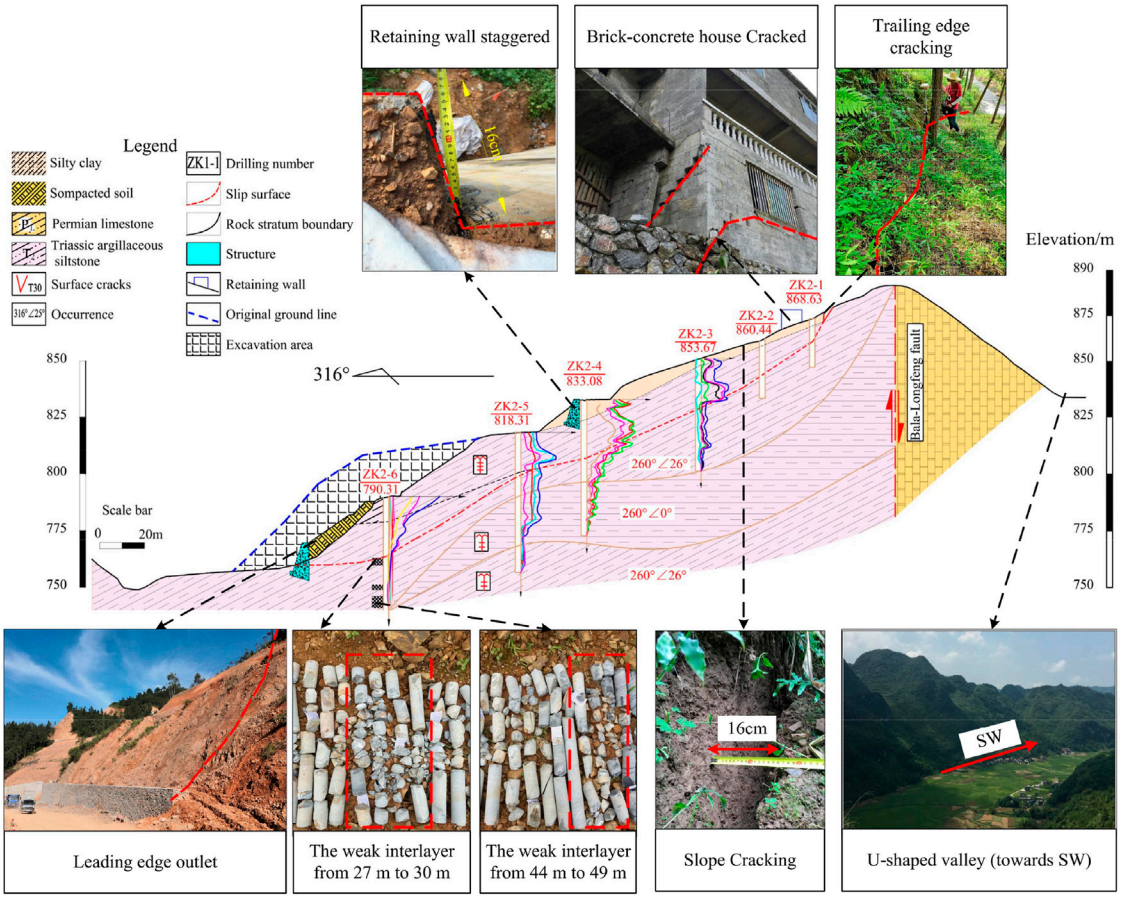

FIGURE 3
Geological profile of the main axis of a typical landslide.

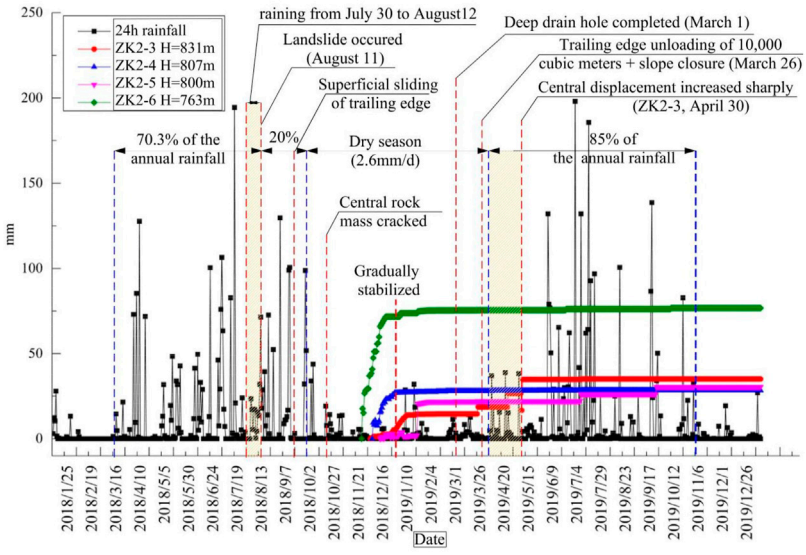

FIGURE 4
Daily rainfall and deep displacement data in the study area.

FIGURE 5
Deformation signs in the middle part entering the dry season.

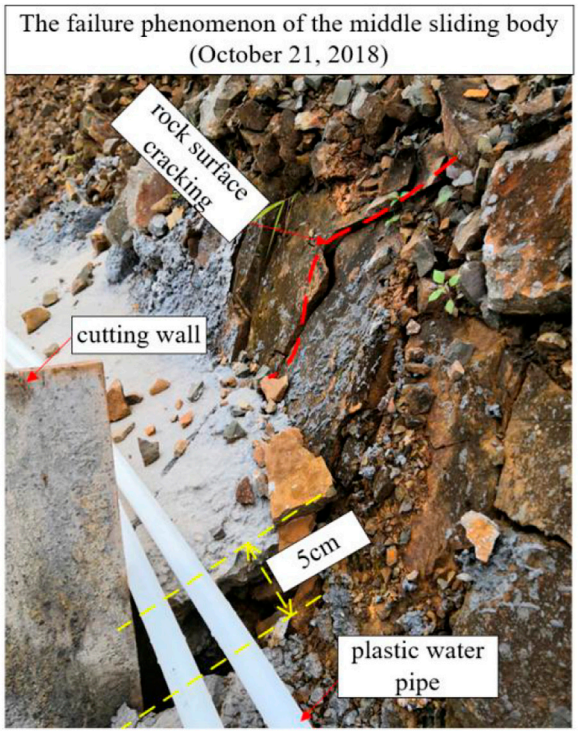

FIGURE 6
Creep remaining after landslide reaction.

In general, the above characteristics show that the landslide is a slipping-stretching ancient landslide formed in geological history.

3.4 Preliminary discussion on the landslide mechanism

Rainfall leads the landslide body to gain weight and decreases the sliding surface shear strength. When the sliding surface shear force is less than the sliding force, a bottom-up deformation occurs: leading edge slips→ newly formed retaining walls in the middle are dragged to the wrong platform→ shallow soil at trailing edge is pulled and cracked by traction. In addition, the slope body is still active in the rainy season after the treatment is completed, indicating that the ancient landslide still inherited its sensitivity to rainfall after the landslide reaction. Therefore, there is good correspondence between landslide reaction development and rainfall. Rainfall is thus the external force in slipping-stretching ancient landslide reaction.

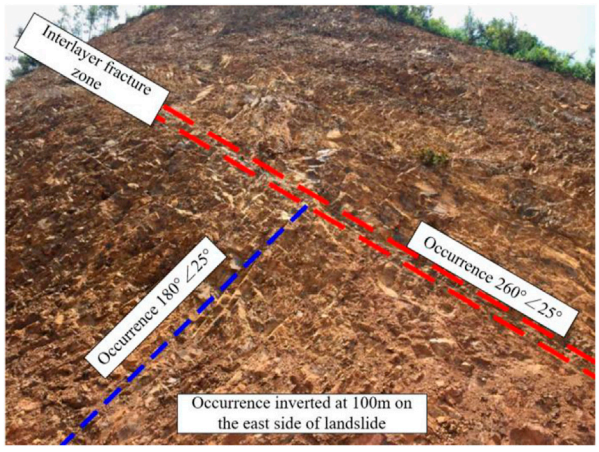

FIGURE 7
Occurrence and interlayer fracture zone on the east side of the landslide area.

4 Analysis of mechanism of slipping-stretching ancient landslide caused by unloading

The Liangtian'ao ancient landslide remained stable for decades, so its original stability coefficient Fs is taken as 1.18. In order to analyze the unloading effect on an ancient landslide reaction, a FEM model was established based on the existing results to analyze the strain characteristics of landslide during the excavation process.

4.1 Numerical model and its parameters

1) Determination for the position of the sliding surface. ZK2-6 has an interlayer broken zone 27 m (760 m) – 30 m (763 m), and a deep displacement monitoring curve change at 763 m. Thus, the sliding surface of the leading edge is located at an elevation of 760 m–763 m. The distribution of the sliding surface is shown in Figure 8.
2) Selection of physical and mechanical parameters. A comprehensive method that combines test evaluation, empirical assessment, and back calculation was used to evaluate the physical and mechanical parameters of the rock and soil. For the underlying bedrock, these parameters have little effect on the results of slope simulation analysis, which can be evaluated directly based on field investigation data. For

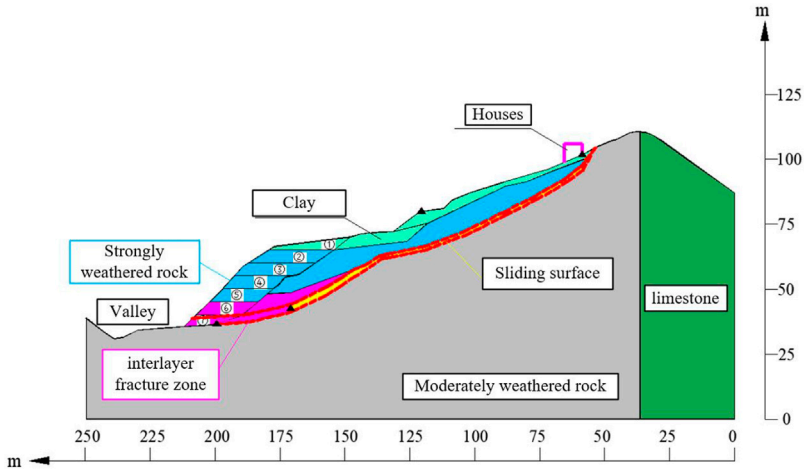

FIGURE 8
Numerical simulation model of the study case.

TABLE 1 Physical and mechanical parameters.

Material	E/MPa	υ	γ/kN·m-3	C/kPa	Φ/(°)
Clay	80	.35	18.7	11.0	16.0
Strongly weathered rock	120	.25	23.0	45.0	28.0
Moderately weathered rock	20,000	.25	26.5	150	45.0
Sliding surface	100	.3	21.0	25.0	15.8
Limestone	30,000	.20	26.5	200	55.0
Interlayer fracture zone	100	.35	23.0	20.0	25.0

residual soil—interlayer zone and sliding surface—key parameters such as modulus and strength are calculated by a back analysis method according to the parameter interval provided by laboratory tests. According to the consistency requirements of landslide failure characteristics, stability coefficient in each excavation stage of landslide simulation analysis, and actual working conditions, the rock and soil conforms to the Mohr-Coulomb model, with the parameters under saturated conditions shown in Table 1. The displacement of the left and right model boundary is fixed in the *X*-direction, and the bottom constrains the displacement in the XY-direction. GEO5 software was used for this calculation.

3) Simulation results. In vertical view, the equivalent plastic strain zone gradually expands from top to bottom with the excavation process, and the leading rock blocks the expansion while the excavation is completed. Taking half of the unloading height as a boundary, the expansion is not obvious when it is less than this value. In contrast, when it exceeds half, the expansion rapidly accelerates to the front edge of the landslide. During the excavation process, the slope deformation proceeds from back to front. When the unloading height of the leading edge reaches half, the middle sliding surface is completely formed. When the unloading height of the leading edge reaches 25 m, the rock mass at the leading edge is deformed, and the influence range spreads 27–30 m below the surface. At the same time, Fs decreases 1.18–0.998 with the excavation time step. Overall, the deformation characteristics of the landslide extend from bottom to top.

4.2 Reaction mechanism of slipping-stretching ancient landslide reaction

As shown in Figure 9. The slipping-stretching ancient landslide remains stable before excavation, and the original sliding surface produces strain with the unloading process acting on the leading edge; at the same time, the stability of the ancient landslide gradually decreases. As gradual cutting at the leading edge support and slope stress is adjusted, the original sliding surface strain cumulates to a qualitative change, leading to a sudden ancient landslide reaction. The reaction is manifested as a chair-shaped crack on the back edge and a subsidence gap cracked onto retaining wall. The weathered rock mass in the front edge blocks the whole from sliding, leading to fewer signs of on-site deformation— consistent with on-site observations. The slipping-stretching landslide is still sensitive to rainfall; with a heavy rainfall season, even a secondary landslide will deform.

Based on these results, the geological background is the internal cause for the formation of slipping-stretching ancient landslides. Landslide reaction is caused by external causes like excavation, with rainfall as the internal cause.

4.3 Principles of treatment for slipping-stretching ancient landslide reactions

The reaction in this study case is mainly related to the unloading effect and rainfall touch-slip effect. The integrity and shear strength

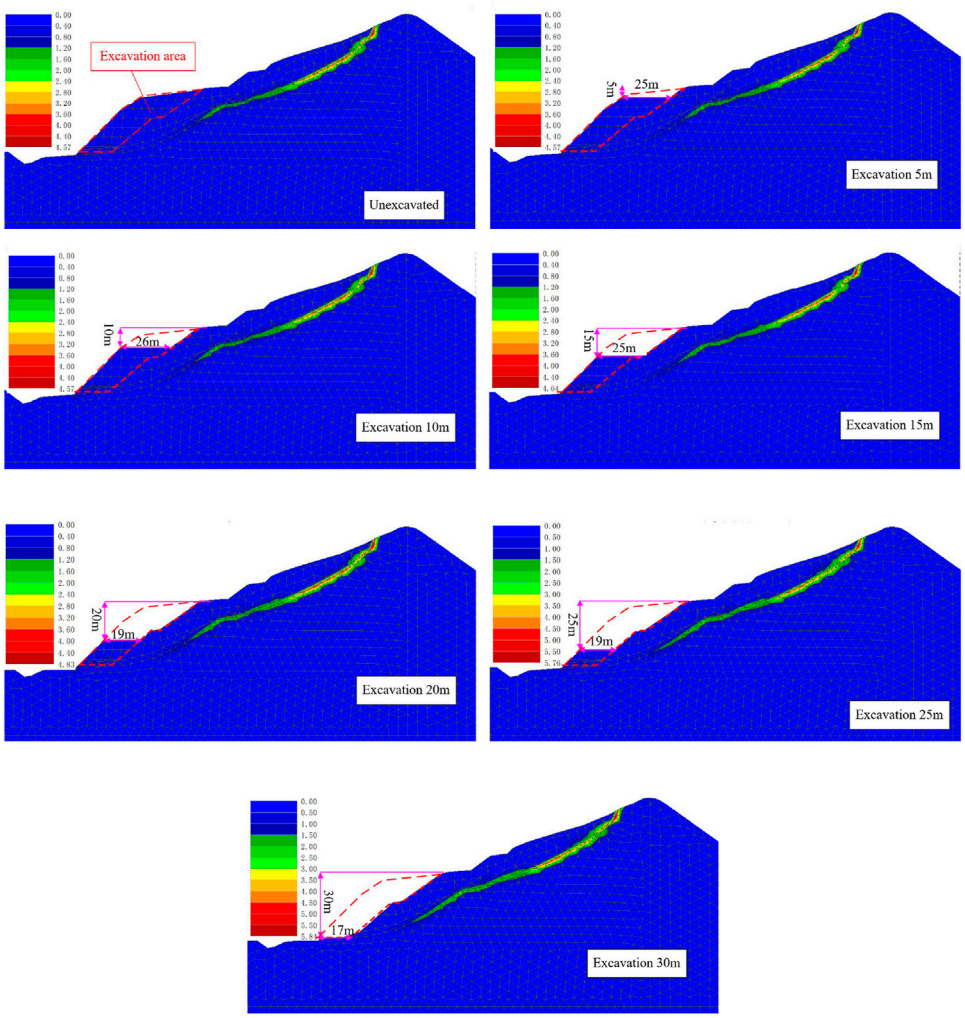

FIGURE 9
Equivalent plastic strain distribution map during excavation.

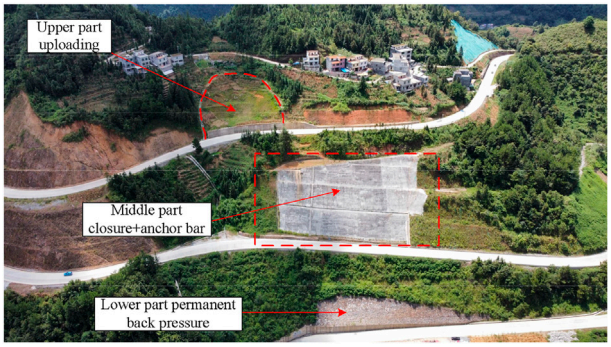

FIGURE 10
Aerial photograph of landslide after treatment (October 2021).

of the leading-edge anti-slip segment affects whether deformation and damage continue to develop. Moreover, rainfall has great significance. The principles governing such landslides can thus be derived.

1) The primary requirements that ensure the stability of the whole slope are control of the thickness of the passively compressed rock mass at its leading edge, and the distance between the excavation surface and the leading edge. As the base support for the slope is cut off, the shear strength of the original sliding surface cannot provide sufficient resistance to sliding.
2) Once a slipping-stretching ancient landslide is revived, it is extremely important to maintain the stability of the passively compressed section at leading edge to control the overall deformation, thereby effectively controlling the downward trend.
3) The different parts of slipping-stretching ancient landslides have various deformed states, and the best time for treatment occurs at the stage of gradual stabilization. For example, the Liangtian'ao landslide unloaded 10,000 m^3 (1/20 of the sliding volume) to stop the landslide downtrend completely.
4) Rainfall is unfavorable to the stability of slipping-stretching ancient landslides, and this type of landslide still inherits the above characteristics after its reaction. In the treatment plan, the rainfall should be cut off as much as possible, and the groundwater should be drained. For example, after the Liangtianao landslide, groundwater was drained and slope

surface was closed so that the threat of re-sliding was avoided during the 2019–2021 rain season (Figure 10).

5 Conclusion

1) The geological background and deformation characteristics indicate that the failure-type of the Liangtian'ao ancient landslide is slipping-stretching, but the ancient macroscopic characteristics are not obvious, and attention should be paid to screening such a landslide in engineering construction.
2) Unloading is the factor that induces a slipping-stretching ancient landslide reaction, and heavy rainfall is the external factor. The slope deformation characteristics advance from bottom to top during the reaction process. Such a landslide still inherits sensitivity to rainfall after reactivation, and rainfall may trigger a secondary reaction.
3) The intact rock mass at the leading edge prevents an overall slide, so its minimum thickness should be controlled during excavation, with attention to the distance between the excavation surface and front rock mass.
4) In treating a slipping-stretching landslide reaction, disturbance to the intact rock mass at the leading edge should be avoided, and the downhill section should be properly unloaded. It is always beneficial to keep the landslide stable by preventing the unencumbered entry of rain into the slope.
5) Due to the restriction of site conditions, the variation law of the Liangtianao landslide in rainfall infiltration was not obtained, and much work is still needed to evaluate the rainfall touch-slip effect on the whole processes of slipping-stretching ancient landslide reactions.

Data availability statement

The original contributions presented in the study are included in the article/Supplementary Material, and further inquiries can be directed to the corresponding author.

Author contributions

LY, drafting papers. ZH (corresponding author), work concept or design, make important revisions to the paper, approve the final paper to be published. LS, HL, LH, and WX, data collection.

Conflict of interest

LY, ZH, HL, LH, and WX were employed by Guangxi Transportation Science and Technology Group Co., Ltd.

The remaining author declares that the research was conducted in the absence of any commercial or financial relationships that could be construed as a potential conflict of interest.

Publisher's note

All claims expressed in this article are solely those of the authors and do not necessarily represent those of their affiliated organizations, or those of the publisher, the editors, and the reviewers. Any product that may be evaluated in this article, or claim that may be made by its manufacturer, is not guaranteed or endorsed by the publisher.

References

Broadbent, C. D., and Ko, K. C. (1971). In Proceedings of the 13th Symp on Rock Mechanics, Urbana, Illinois, September 1971, 537–572.

Burda, J., Hartvich, F., Valenta, J., Smítka, V., and Rybář, J. (2013). Climate-induced landslide reactivation at the edge of the Most Basin (Czech Republic)–progress towards better landslide prediction. *Nat. Hazards Earth Syst. Sci.* 13 (2), 361–374. doi:10.5194/nhess-13-361-2013

Cai, Y. J., Xu, F. X., Zhu, M., Li, Y. H., and Gao, J. H. (2021). Risk analysis of instability and blockage of the residual body of the Baige landslide on the Jinsha River. *Eng. Sci. Technol.* 53 (06), 33–42. (in Chinese).

Chen, X. L., Hui, H. J., and Zhao, Y. H. (2014). The relationship between fault properties and landslide distribution: Taking the large-scale landslide in the Wenchuan earthquake as an example. *Seismol. Geol.* 36 (2), 358–367. (in Chinese).

Deng, H., Wu, L. Z., Huang, R. Q., Guo, X. G., and He, Q. (2017). formation of the siwanli ancient landslide in the dadu river, China. *Landslides* 14 (1), 385–394. doi:10.1007/s10346-016-0756-9

Huang, R. Q. (2009). Some catastrophic landslides since the twentieth century in the southwest of China. *Landslides* 6 (1), 69–81. doi:10.1007/s10346-009-0142-y

Huang, X. H., Yi, W., Gong, C., Huang, H. F., and Yu, Q. (2020). Research on the deformation mechanism of ancient landslides caused by excavation. *Chin. J. Geotechnical Eng.* 42 (7), 1276–1285. (in Chinese).

Huang, X., Yang, W. M., Zhang, C. S., Shen, J. F., and Liu, T. (2013). Deformation characteristics and formation mechanism of Xieliupo landslide in Zhouqu. *J. Geomechanics* 19 (2), 178–187.

Li, M. H., Zheng, W. M., Shi, S. W., and Xie, Z. S. (2008). The revival mechanism and stability analysis to Jiaju landslide of Danba county in Sichuan province. *J. Mt. Sci.* 26 (5), 577–582. (in Chinese).

Li X, X., Li, S. D., Chen, J., and Liao, Q. L. (2008). The internal and external dynamic coupling mechanism of geological disasters. *Chin. J. Rock Mech. Eng.* (9), 1792–1806. (in Chinese).

Liu, N. F., Li, N., Li, G. F., and Song, Z. P. (2022). Method for evaluating the equivalent thermal conductivity of a freezing rock mass containing systematic fractures. *Rock Mech. Rock Eng* doi:10.1007/s00603-022-03038-9

Liu, N. F., Li, N., Wang, S. J., Li, G. F., and Song, Z. P. (2022). A fully coupled thermo-hydro-mechanical model for fractured rock masses in cold regions. *Cold Regions Sci. Technol.* 205, 103707. doi:10.1016/j.coldregions.2022.103707

Lo, K. Y., Wai, R. S. C., Palmer, J. H. L., and Quigley, R. M. (1978). Time-dependent deformation of shaly rocks in southern Ontario. *Can. Geotechnical J.* 15 (4), 537–547. doi:10.1139/t78-057

Macciotta, R., Hendry, M., and Martin, C. D. (2016). Developing an early warning system for a very slow landslide based on displacement monitoring. *Nat. Hazards* 81 (2), 887–907. doi:10.1007/s11069-015-2110-2

Pradhan, S., Toll, D. G., Rosser, N. J., and Brain, M. J. (2022). An investigation of the combined effect of rainfall and road cut on landsliding. *Eng. Geol.* 307, 106787. doi:10.1016/j.enggeo.2022.106787

Qu, S. J., Zhao, J. J., Ding, X. M., Xie, M. L., and Bu, F. (2016). Discrete element simulation of rainfall-induced gently dipping bedding landslide mechanism. *Hydrogeology Eng. Geol.* 43 (6), 120–126. (in Chinese).

Sangirardi, M., Amorosi, A., and de Felice, G. (2020). A coupled structural and geotechnical assessment of the effects of a landslide on an ancient monastery in Central Italy. *Eng. Struct.* 225, 111249. doi:10.1016/j.engstruct.2020.111249

Song, L., Zuo, S. S., Ding, J., Zhong, H. J., Zhang, H., et al. (2012). Analysis of the cause and mechanism of the resurrection of the hongmei village landslide in dujiangyan, sichuan. *Chin. J. Geol. Hazard Control* 23 (2), 34–37. (in Chinese).

Wartman, J., Montgomery, D. R., Anderson, S. A., Keaton, J. R., Benoît, J., dela Chapelle, J., et al. (2016). The 22 March 2014 oso landslide, Washington, USA. *Geomorphology* 253, 275–288. doi:10.1016/j.geomorph.2015.10.022

Wei, C. L., Zhang, Y., Feng, W. K., et al. (2018). Genesis and reactivation analysis of large-scale ancient landslides in the meandering section of the upper minjiang river—taking yuanbazi ancient landslide in songpan county as an example. *Hydrogeology Eng. Geol.* 45 (6), 141–149. (in Chinese).

Wolken, G. J., Liljedahl, A. K., Brubaker, M., Coe, J. A., Fiske, G., Christiansen, H. H., et al. (2021). *Arctic report card*.Glacier and permafrost hazards

Wu, R. A., Zhang, Y. S., Guo, C. B., Yang, Z. H., Ren, S. S., and Chen, P. (2018). Study on the resurrection characteristics and risk prediction of the Shangyaogou ancient landslide in Songpan, Western Sichuan-Wu Ruian. *Chin. J. Geotechnical Eng.* 40 (9), 1659–1667. (in Chinese).

Xue, D., Li, T., Wei, Y., and Gao, M. (2015). Mechanism of reactivated badu landslide in the badu mountain area, southwest China. *Environ. Earth Sci.* 73 (8), 4305–4312. doi:10.1007/s12665-014-3714-7

Zhang C, C., Yin, Y., Yan, H., Li, H., Dai, Z., and Zhang, N. (2021). Reactivation characteristics and hydrological inducing factors of a massive ancient landslide in the three Gorges Reservoir, China. *Eng. Geol.* 292, 106273. doi:10.1016/j.enggeo.2021.106273

Zhang, X., Zhou, H. L., Liu, F., Yu, F., and Xie, C. T. (2021). Research on the characteristics of temperature changes in Tian'e in the past 60 years. *Agric. Disaster Res.* 11 (8), 73–75+8. (in Chinese).

Zhang, Y. W., Fan, S. Y., Yang, D. H., and Zhou, F. (2022b). Investigation about variation law of frost heave force of seasonal cold region tunnels: A case study. *Front. Earth Sci.* 9, 806843. doi:10.3389/feart.2021.806843

Zhang, Y. W., Song, Z. P., and Weng, X. L. (2022a). A constitutive model for loess considering the characteristics of structurality and anisotropy. *Soil Mech. Found. Eng.* 59 (1), 32–43. doi:10.1007/s11204-022-09781-z

Zhang, Z. Y. (2016). *The principle of engineering geological analysis*. 4th. Kolkata India: Geological Press. (in Chinese).

Zhong, Y. J., Fan, X. M., Dai, L. X., Zhou, C. B., Zhang, F. Y., and Xu, Q. (2021). Research on the giant ancient landslide in Diexi on the minjiang river. *Prog. Geophys.* 36 (4), 1784–1796. (in Chinese).

Zou, Z. X., Tang, H. M., Xiong, C. G., Wu, Y. P., Liu, X., and Liao, S. B. (2012). Progressive failure geomechanical model and stability analysis of large bedding rock landslides. *Chin. J. Rock Mech. Eng.* 31 (11), 2222–2231. (in Chinese).